# Patterning Metallic Nanostructures by Ion-Beam-Induced Dewetting and Rayleigh Instability

**ARTICLE** *in* NANO LETTERS · JUNE 2006

Impact Factor: 13.59 · DOI: 10.1021/nl060492z · Source: PubMed

NANO LETTERS

2006
Vol. 6, No. 5
1047−1052

# Patterning Metallic Nanostructures by Ion-Beam-Induced Dewetting and Rayleigh Instability

**Jie Lian,*,† Lumin Wang,† Xiangcheng Sun,† Qingkai Yu,‡ and Rodney C. Ewing†**

*Department of Geological Sciences, Department of Materials Science & Engineering, and Department of Nuclear Engineering & Radiological Sciences, University of Michigan, Ann Arbor, Michigan 48109, and Texas Center of Advanced Materials, Department of Electrical and Computer Engineering, University of Houston, Houston, Texas 77081*

*Received March 2, 2006; Revised Manuscript Received April 11, 2006*

**ABSTRACT**

**Alternative fabrication and patterning of ordered nanostructures has become critically important as the size of devices reaches the nanoscale and the resolution of conventional optical lithography approaches its physical limit. Here, we have developed a simple method that allows one to pattern metallic surface nanostructures with precisely controlled size, spacing, and location using ion-beam-induced dewetting and Rayleigh instability. Predefined patterns by focused ion beam direct-writing were used as the templates for the self-organization of ordered nanostructures. Single or double chains, concentric rings, and two-dimensional arrays of metallic nanoparticles with a well-controlled spacing, diameter, and location were fabricated. This approach represents a maskless process that combines the top-down and bottom-up patterning methods, and no chemical etching or pattern transfer steps are involved. This method can be applied to many metallic systems in constructing complex, higher-order functional nanostructures for numerous applications such as data storage, nanocatalytic systems, and templated fabrication of ordered nanostructures.**

Fabricating functional structures in a variety of materials with specific patterns is critical to the development of microelectronic devices and data storage technologies. The fabrication methods used in the microelectronics industry, particularly photolithography, will soon reach their fundamental physical limit. Alternative approaches for creating surface patterns in a controllable and repeatable manner have been extensively studied, and the controlled patterning of nanostructures has been achieved in predefined templates fabricated by "top-down" approaches. A variety of alternative methods have been developed for patterning nanostructures, such as advanced photolithographic techniques utilizing extreme ultraviolet[1] or hard X-ray radiation as the light sources,[2] soft lithography[3] and replica molding,[4] micro-contact[5] and nanoimprinting,[6,7] direct-writing methods by e-beam[8] and ion beam,[9] and dip-pen nanolithography.[10] In contrast to top-down methods, "bottom-up" methods assemble the atomic or molecular constituents into organized surface structures, and it is highly desirable to develop alternative approaches for the bottom-up fabrication of functional nanostructures and patterns by self-assembly processes at well-defined surfaces that have been created using top-down methods.

* Corresponding author. E-mail: jlian@umich.edu. Phone: 734-647-5704. Fax: 734-647-5706.
† University of Michigan.
‡ University of Houston.

10.1021/nl060492z CCC: $33.50 
**Published on Web 04/22/2006**

Metallic thin films deposited on solid substrates are typically thermodynamically unstable at elevated temperatures,[11−13] and dewetting will occur upon heating if the surface energy of the metal, $\gamma_m$, is greater than one-half the work of adhesion, $w_{ad}$, in which a finite contact angle between the film and substrate is energetically favorable.[14] Dewetting has been reported for a variety of metallic films on a silica substrate upon heating, such as Au, Cu, and Ni.[15] Minimization of the free energy of the system in the thin film geometry allows the dewetting process to act as a structure-directing mechanism, and the interplay between dewetting and phase separation provides the possibility for nanoscale patterning of the surface via a self-assembly process. Anisotropic spinodal dewetting as a route for self-assembly of surface patterns has been realized in a polymer film.[16] Well-aligned stripe patterns of gold and silver nanoparticles have been self-assembled by dewetting a dilute film of polymer-coated nanoparticles floating on a water surface.[17] Following these ideas, we create various patterns of one- or two-dimensional arrays of metallic nanoparticles via ion-beam-induced dewetting and Rayleigh instability processes.

We first report the phenomena of ion-beam-induced dewetting of a Co thin film (∼25 nm). The Co thin film was deposited on Si(100) substrates at room temperature in

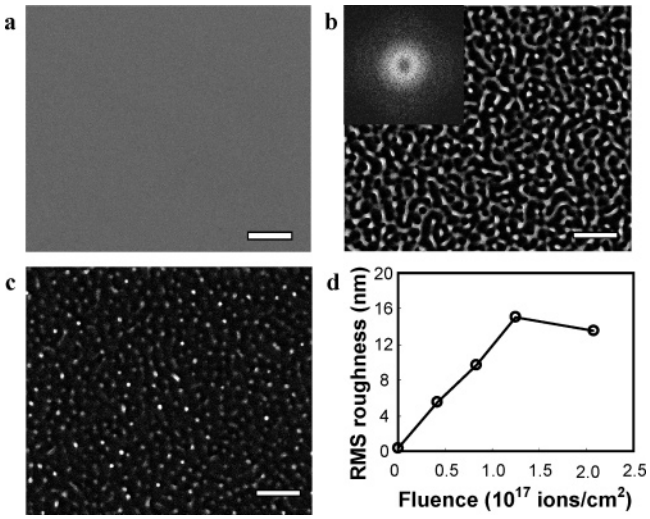


**Figure 1.** Ion-beam-induced dewetting of a Co thin film deposited on Si wafers with a native oxide layer. (a−c) SEM images showing morphological evolution of the Co thin film under 30-keV $Ga^+$ ion bombardment at different fluences: original (a); $1.26 \times 10^{17}$ ions/cm$^2$ (b); and $2.08 \times 10^{17}$ ions/cm$^2$ (c). The well-defined ring pattern of the Fourier transformed image of the dewetted structure (inset in part b) displays a characteristic length scale, while the radial symmetry of the transformed image indicates the isotropy of the dewetted pattern. (d) The root-mean-square (rms) surface roughness, analyzed from corresponding AFM images, as a function of ion fluences. Scale bars = 1 $\mu$m.

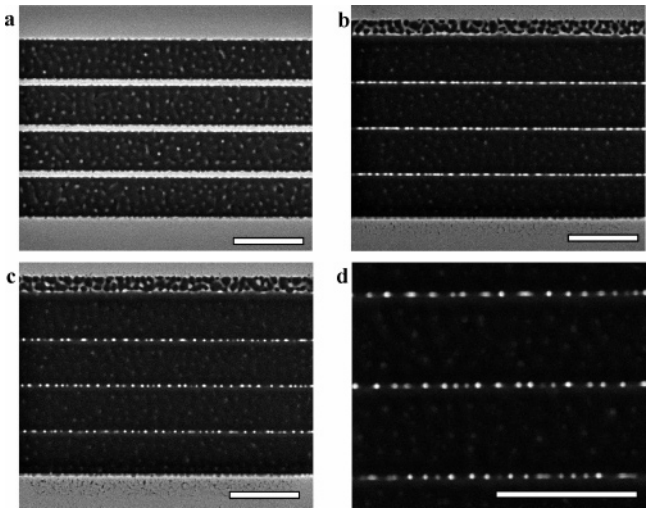


**Figure 2.** Formation of single chains of Co nanoparticles induced by Rayleigh instability. (a−c) SEM images showing the morphology and geometry evolutions of Co stripes predefined by FIB direct-writing upon ion bombardment at different fluences: before ion bombardment (a); $8.37 \times 10^{16}$ ions/cm$^2$ (b), and $1.04 \times 10^{17}$ ions/cm$^2$ (c). (d) A closeup of (c) showing single chains of Co nanoparticles induced by Rayleigh instability. Scale bars = 2 $\mu$m.

an ultrahigh vacuum magnetron sputtering chamber (with a base pressure in the $10^{-9}$ Torr range). The sputtering conditions were Ar pressure 7.5 mTorr, dc power 120 W, and target-to-substrate distance 13 cm. The surface of the Si wafer was degreased before thin film deposition. The microstructure analysis of Co thin film was performed using analytical transmission electron microscopy (TEM), JEOL 2010F, with a field emission source operated at 200 kV. A native oxide of silica with the thickness of 2−3 nm was identified between the Co thin film and Si wafer (Figure S1, Supporting Information). The ion bombardment experiments were performed using a field emission scanning electron microscope/focused ion beam (SEM/FIB) dual beam system (FEI Nova 200 NanoLab). A 30-keV focused $Ga^+$ beam normal to the thin film surface was used for ion sputtering, and the beam current was fixed at 100 pA for all of the ion beam experiments. The spot size of the 30 keV $Ga^+$ ion beam is 23 nm. The ion beam was scanned across areas predetermined on the sample surface. The topography of patterned structures was measured using atomic force microscopy (Nanoscope IV) operated at a tapping mode using phosphorus-doped Si cantilevers. Before ion bombardment, the Co thin film is featureless (Figure 1a). Upon 30-keV focused $Ga^+$ ion irradiation, the Co thin film began to dewet and a partially connected patterned structure appeared (Figure 1b). The surface structure coarsened; thus, the surface roughness increased upon ion bombardment. A further increase in the ion fluence led to the formation of nanoparticles distributed randomly on the substrate (Figure 1c). Eventually, metallic Co nanoparticles were sputtered away due to the energetic beam bombardment, and the surface roughness decreased correspondingly as a result of a nanosmoothing process (Figure 1d).

The surface energy of liquid cobalt ($\gamma_{Co}$) at the melting temperature (1768 K) is 1.93 N/m with a negative temperature coefficient of −0.33 mN/mK.[18] The surface energy of silica ($\gamma_{SiO_2}$) is 0.278 N/m at 1273 K with a temperature coefficient of 0.035 mN/mK.[19] On the basis of the surface energy differences, dewetting may occur for a Co thin film on the silica substrate under equilibrium conditions. The pattern formation of a Co film on silica can be attributed to ion-beam-induced dewetting, in which the energy deposition upon energetic ion bombardment causes local heating of the metal films and atomic displacement. A thermal spike can be produced upon high energy deposition in the metallic thin film, leading to the formation of craters or holes as a result of atom depletion along the original track of the ions.[20,21] These may drive the metastable thin film toward equilibrium and lead to dewetting upon ion bombardment.

Three Co stripes (Figure 2a) with a width of ∼200 nm and a spacing of 1.2 $\mu$m used as templates were created first via FIB direct-writing. The space and width of the Co stripes can be controlled easily by FIB milling in well-defined positions. Uniformly scanned ion bombardment was then performed. Ion beam sputtering causes a decrease in the width of Co stripes, and at a fluence of $8.37 \times 10^{16}$ ions/cm$^2$, the width of Co stripes was thinned down to ∼54 nm (Figure 2b). Fragmentation of nanowires occurred with the fragments having typical lengths of several hundred nanometers. Nanowires continued to breakdown into linear chains composed of Co nanoparticles upon further ion irradiation. The average spacing and diameter of the Co nanoparticles are ∼256 and 58 nm, respectively. The average height of nanoparticles is estimated to be ∼63 nm, as measured from the SEM image tilted to 52°. Therefore, the aspect ratio of

nanoparticles is close to 1, suggesting the nanosphere morphology of these nanodroplets.

The fragmentation of the Co stripes upon ion beam bombardment to a chain of nanodroplets can be explained to be a result of Rayleigh instability. A continuous nanowire may decay by minimizing interfacial energy during thermal annealing. Harmonic perturbation of the wire radius lowers its interfacial energy such that the wire breaks down into a row of spherical droplets when the wavelength ($\lambda$) of wire perturbation is larger than the circumference of the wire (radius $r$), $\lambda > 2\pi r$.[22] A large variety of phenomena, such as the instability of liquid jets, atomic nuclei, or liquid droplets, are due to Rayleigh instability.[23] Linear instability also revealed a fast growth rate of $\lambda$m of radius fluctuations during the initial stage of fragmentation, depending on specific mass-transport mechanisms. For surface diffusion, a value of $\lambda m = 8.89r$ was predicted.[24] An average droplet diameter $d_{\text{cluster}}$ is estimated to be: $d_{\text{culster}} = 3.78r$. Rayleigh instability may not occur for the wires with larger diameters due to kinetic limitations.[25] Before ion beam bombardment, the Co stripes with a width of ~200 nm were created, and the thickness of Co stripes should be slightly larger than that of the original Co thin film (~25 nm) because of dewetting and atom redeposition. Ion beam bombardment thinned down the width of the Co stripes, and the redeposition of Co atoms may change the geometry of Co stripes to nanowires. Assuming that the Co wires are cylinders, the diameter of the nanowire is close to 54 nm before fragmentation (Figure 2b). Therefore, the ratio (9.48) between the average spacing of nanoparticles and the radius of nanowire before fragmentation is consistent with the theoretical value of 8.89, as predicted by Nichols and Mullins[24] for decay of a 54 nm diameter wire. This result clearly demonstrates that the fragmentation of Co nanowires and the formation of nanochains observed in Figure 2 result from Rayleigh instability. Unlike the morphological instability of nanowires upon thermal annealing in which the volume of nanowires is assumed to be conservative, continuous ion beam milling will sputter the Co atoms away, and thus the diameter of Co nanoparticles (~58 nm) is expected to be smaller than that predicted by theory.

The metallic surface nanostructure patterns induced by dewetting and Rayleigh instability are tunable by controlling the shape and size of the templates predefined by FIB direct-writing. Figure 3a shows four Co stripes with varying widths of 200, 300, 400, and 500 nm, respectively. Similar to that observed for the 200 nm Co stripes (Figure 2), ion beam sputtering causes the shrinkage of Co stripes with the widths of 200 and 300 nm and changes the geometry of Co stripes to Co nanowires as a result of atom redeposition. A prominent feature is that the shrinkage of Co stripes starts first from the edge of the stripes; thus, the Co nanowires are well positioned at the center of Co stripes (Figures 2 and 3). The variation in the geometry leads to much different sputter yields between the edge and center of Co stripes. Sputtering yields are usually higher with larger ion beam incident angles,[26] and thus atoms are more easily sputtered away because of the off-normal geometry for the edge of stripes

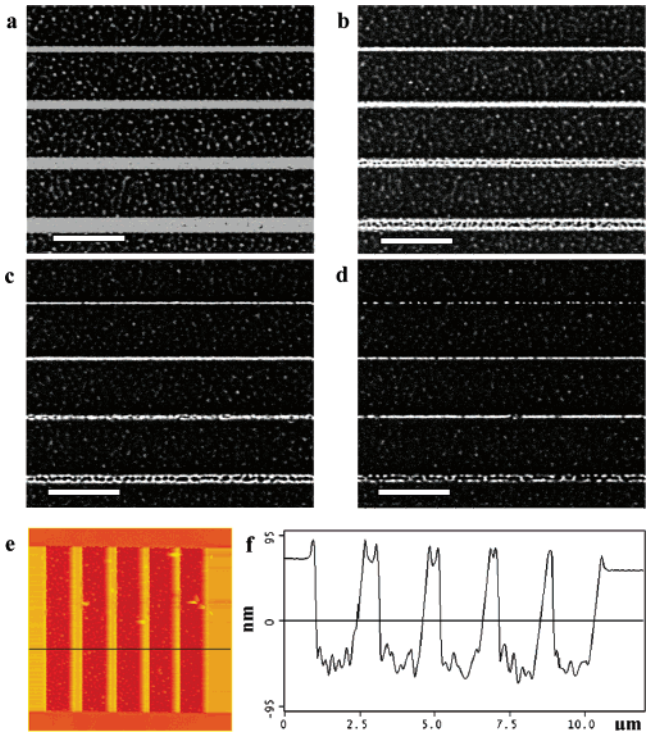


**Figure 3.** Nanostructure patterns are controllable by varying the shape and size of the templates predefined by FIB direct-writing. (a) A scanning ion beam image of four Co stripes with varying widths of 200, 300, 400, and 500 nm. (b−d) Snapshots from a movie to record the detailed morphological evolution of Co stripes upon ion bombardment. The corresponding ion fluences are $3.0 \times 10^{16}$ (b), $6.82 \times 10^{16}$ (c), and $10.6 \times 10^{16}$ ions/cm$^2$ (d), respectively. Double chains of Co nanoparticles were patterned on the 500 nm Co stripes by ion-beam-induced dewetting and Rayleigh instability. (e, f) An AFM image and corresponding section analysis showing the morphology variation for Co stripes with different widths. Scale bars = 2 $\mu$m. The scanning area of (e) is 12 $\mu$m by 12 $\mu$m.

relative to the incident ion beam normal to the thin film surface. Interestingly, a completely different evolution of the morphology was observed for the Co stripes with larger widths (400 and 500 nm), despite the similar shrinkage of stripe widths upon ion bombardment. Above a certain ion fluence (e.g., $\sim 3 \times 10^{16}$ ions/cm$^2$), the Co stripes broke down to two nanowires (Figure 3b). Dewetting occurred in the areas between two nanowires. For the 400 nm Co stripe, two nanowires merged into a single nanowire due to the relatively small spacing between them before the fragmentation caused by the Rayleigh instability (Figure 3c). In contrast, for the 500 nm width Co stripe, double chains of Co nanoparticles were observed (Figure 3d). Eventually, all of the Co nanoparticles were sputtered away upon further ion milling.

We performed atomic force microscopy (AFM) measurements of the Co stripes before ion milling (Figure 3e). Sectional analysis (Figure 3f) clearly demonstrates the variation of topography of the Co stripes. Specifically, rim morphology with a height of ~20 nm along the edges of milled boxes was created during the fabrication of Co stripes by FIB direct-writing. Ion-beam-induced dewetting may contribute partially to the buildup of the rim structure. Most likely, atom redeposition to the edges of the milled box,

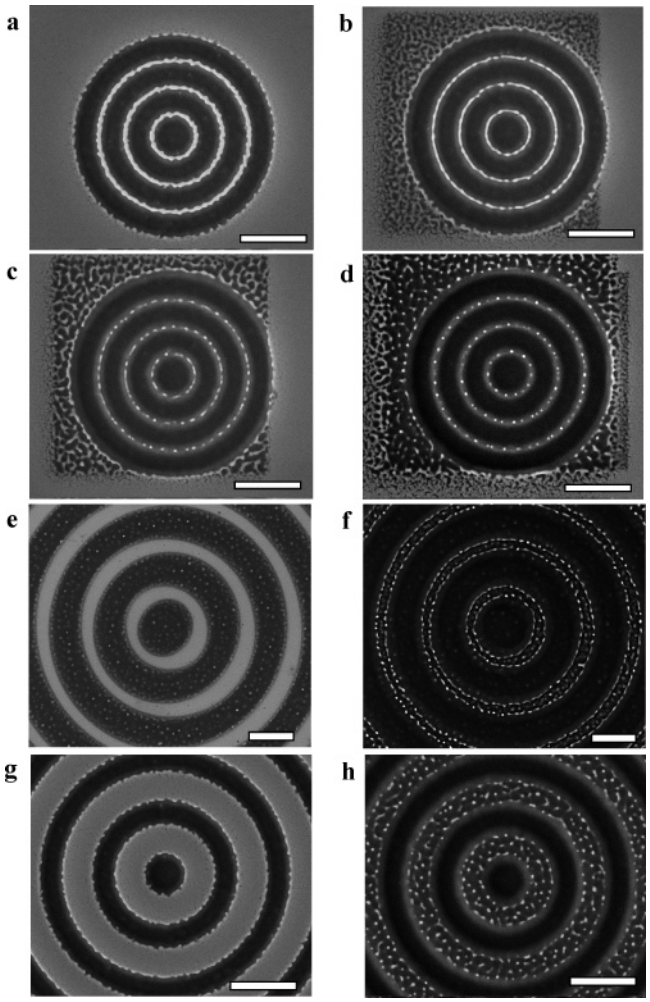


**Figure 4.** The concentric nanoring patterns induced by Rayleigh instability. (a−d) SEM images showing the morphological evolution of concentric stripes with width of 150 nm and the formation of nanoring patterns at different ion fluences: original (a); $4.16 \times 10^{16}$ (b); $8.32 \times 10^{16}$ (c); and $10.4 \times 10^{16}$ ions/cm$^2$ (d). The average diameter and spacing of Co nanoparticles in (d) are ∼67 and ∼320 nm, respectively. (e, g) SEM images showing concentric stripes fabricated by FIB direct-writing with the widths of ∼670 and 900 nm, respectively. (f, h) Patterned structures of (e) and (g) at an ion fluence of $1.25 \times 10^{17}$ ions/cm$^2$. Scale bars = 2 $\mu$m.

which is typically observed during the FIB ion milling process, leads to the elevated rim structures above the original Co thin films. The heights of rims for Co stripes of 500, 400, and 300 nm widths are ∼26, 18, and 10 nm, respectively (Figure 3f). Classical Sigmund theory indicates that the sputtering yield is surface curvature dependent, and the sputtering rate is faster for a concave surface as compared with that of convex surface.[27] The variation in the morphology results in significantly lower sputtering yields for rims of the Co stripes, and thus the Co stripes break down to two well-aligned nanowires along the rims for 400 and 500 nm Co stripes. Further ion irradiation leads to double chains of Co nanodots due to ion-beam-induced Rayleigh instability for the 500 nm Co stripe.

By creation of concentric Co stripes as templates (Figure 4a), nanorings composed of Co nanoparticles were patterned. The details of morphological evolution of concentric Co stripes upon ion beam bombardment are recorded in a video (Supporting Information). Similar to those observed in straight Co stripes (Figure 2), the concentric Co stripes were thinned down to ∼70 nm from an original width of 150 nm before the fragmentation (Figure 4b). The concentric Co stripes breakdown into nanorings of Co nanoparticles upon further ion irradiation. The spacing of the nanoparticles is ∼320 nm, in excellent agreement with the Rayleigh criterion. The average diameter of Co nanoparticles is ∼67 nm (Figure 4d). As the width of the concentric Co stripes predefined by FIB direct-writing increased to 670 nm (Figure 4e), triple rings of Co nanoparticles were patterned with ion beam bombardment (Figure 4f). With a further increase in the width of concentric stripes to 900 nm, randomly distributed Co nanoparticles formed upon ion bombardment (Figure 4h), similar to the dewetted structure of planar Co thin films (Figure 1).

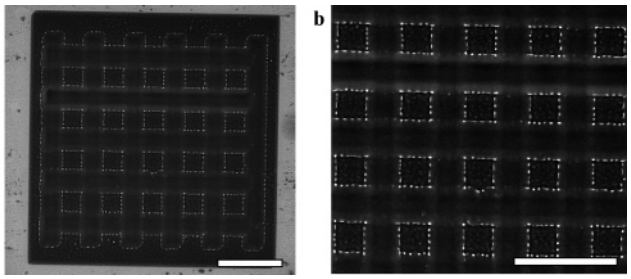


**Figure 5.** A complex pattern induced by ion-beam-induced dewetting and Rayleigh instability. Metallic Co nanoparticles were distributed along the rims of a predefined square pattern created by FIB direct writing upon uniformly scanned ion beam bombardment. Scale bars = 5 $\mu$m.

Figure 5 shows a complex pattern in which metallic Co nanoparticles were distributed along the edge of predefined square patterns created by FIB direct-writing. AFM measurement shows a unique rim morphology of patterned squares, and the formation of Co nanoparticles along the rims again is due to the Rayleigh instability upon uniformly scanned ion beam bombardment. We further demonstrate the possibility of this method for fabricating two-dimensional arrays of metallic nanoparticles with well-controlled spacing and pattern arrangements. Figure 6 shows hexagonal arrays of metallic Co nanoparticles induced by ion-beam-induced dewetting. This pattern was created by uniformly scanned ion beam bombardment on hexagonally arranged Co disks predefined via FIB direct-writing. The original spacing and diameter of Co disks are 700 and 350 nm, respectively. Uniformly scanned ion beam bombardment leads to the formation of hexagonal arrays of Co nanoparticles with reducing diameter to ∼90 nm due to ion beam sputtering, and the pattern follows the location and arrangement of the original template. The height of nanoparticles increases to 91.7 nm due to ion-beam-induced dewetting despite ion sputtering.

FIB-patterned topographies have recently been used as templates for the fabrication of quantum dots in linear chains[28] and periodic two-dimensional lattices[29] by self-assembled MBE growth. Furthermore, one-dimensional arrays of topographical ripples have been created by direct ion

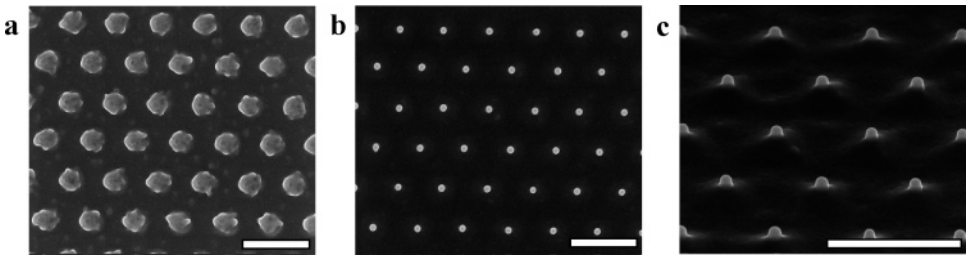


**Figure 6.** Two-dimensional hexagonal arrays of Co nanoparticles created by ion-beam-induced dewetting. (a) The original spacing and diameter of Co disks are 350 nm and spacing of 700 nm, respectively. (b) Uniformly scanned ion beam bombardment at a dose of $1.04 \times 10^{17}$ ions/cm$^2$ leads to the formation of hexagonal arrays of Co nanoparticles with reducing diameter to ~90 nm due to ion beam sputtering, and the pattern follows the location and arrangement of the original template. (c) A 52° view of the hexagonal array of Co nanoparticles. Scale bars = 1 $\mu$m.

beam sputtering on lateral templates created by FIB milling.[30] Instead, the method we report here represents a completely different route for fabricating higher order nanostructures by ion-beam-induced dewetting and Rayleigh instability, and the minimization of the free energy of the system in the thin film geometry acts as the directing mechanism for the self-organization of nanostructures. As compared with typical wet methods in which multisteps, such as lithography, etching, patterning development and transfer, are usually involved, this method delivers a much simpler approach for controlled and reproducible patterning of ordered nanostructure on a wide range of metallic systems (e.g., Co, Fe, Pt). We further demonstrated that some complex patterns and two-dimensional nanoarrays of metallic nanoparticles (Figures 5 and 6), as might be required for the fabrication of higher ordered nanostructures, can be created. The spacing, diameter, and morphology of the metallic nanoparticles can be well controlled by varying the shape, spacing, and arrangement of the templates and ion fluences.

Ion-beam-induced damage and the corresponding compositional and microstructural changes has often been considered as a major limitation for the application of FIB technology, particularly for applications with high ion fluences above $10^{18}$ ions/cm$^2$ (e.g., ion milling).[31] Ballistic mixing becomes important for thin film geometry upon ion bombardment when the thickness of the thin film reduces to several nanometers, which correspond to the size of the collision cascade.[32] A significant change in the magnetic properties has been reported for Pt(3.4 nm)/Co(1.4 nm)/Pt(4.5 nm) film deposited on a sapphire substrate upon 30 keV $Ga^+$ ion bombardment.[31] On the basis of a full cascade calculation using the well-known TRIM code (transport range of ion in matter), the projected range of 30 keV $Ga^+$ in Co layers is estimated to be 9.8 nm with the mean lateral straggling of 5.0 nm (Figure S2, Supporting Information). The peak of collision events occurs at the depth of 6.5 nm, and the sputtering yield is ~7.02 Co atoms/ion. Because a large amount of implanted $Ga^+$ ions will be sputtered away due to the interaction of implanted ions with the substrate, a steady state will be achieved eventually in which the sputtering yield of $Ga^+$ is equal to the implantation yield. [33] The peak concentration of $Ga^+$ ions is within the area between the surface and projected ion range due to the dynamic sputtering process.[34] Thus, atomic displacements and implanted $Ga^+$ ions only occur at the very near surface region (less than 10 nm), which is far above the interface of Co and Si substrate. Therefore, significant ion mixing between Co and Si is not expected in this study. A surface amorphous layer with the thickness of ~40 nm will be created in Si substrate upon 30 keV $Ga^+$ bombardment, while Co nanoparticles will remain crystalline upon ion bombardment due to the high mobility of Co interstitials or the dynamic annealing effects despite of the fact that 760 vacancies were created by each incident ion on the average. Further possibility to reduce the ion beam damage and $Ga^+$ implantations can be achieved by using lower energy focused $Ga^+$ ions or broad inert ion beams (such as $Ar^+$ or $Kr^+$) to provide energy required to drive the ion-beam-induced dewetting and Rayleigh instability processes for patterning higher ordered nanostructures.

In summary, we have developed a simple method that allows one to pattern metallic surface nanostructures by ion-beam-induced dewetting and Rayleigh instability processes. The template morphology, ion beam sputtering, and the interplay between dewetting and Rayleigh instability define the location, shape, size, spacing, and pattern arrangements of the nanostructures. For specific regimes of thin widths, Rayleigh instability is dominant, and ion-beam-induced dewetting and sputtering processes only remove the film. As the shape of the templates changes or the template size increases, patterned structures may be mainly controlled by the dewetting process. Further flexibility can be achieved by depositing desired metallic films through masks by conventional optical lithography and patterning surface nanostructures over large areas via dewetting and Rayleigh instability upon heating or using broad beam irradiations.

**Acknowledgment.** This work was supported by the Office of Basic Energy Sciences of the U.S. Department of Energy (DE-FG02-97ER45656 and DE-FG02-02ER46005) and the NSF NIRT program (EAR-0309772).

**Note Added after Print Publication.** On p 1047, the name of one of the authors is misspelled in the version posted on the Web April 22, 2006 (ASAP), and published in the May 2006 issue (Vol. 6, No. 5, pp 1047−1052); the correct electronic version of the paper was published on November 8, 2006, and an Addition and Correction appears in the November 2006 issue (Vol. 6, No. 11).

**Supporting Information Available:** A video showing detail of the morphological evolution of concentric Co stripes upon ion beam bombardment, Figure S1 showing the microstructure of a Co thin film deposited on a Si wafer with a native oxide, and Figure S2 showing damage events and ion distributions of 30 keV $Ga^+$ in a Co layer. This material is available free of charge via the Internet at http://pubs.acs.org.

## References


(1) Gwyn, C. W.; Stulen, R.; Sweeney, D.; Attwood, D. *J. Vac. Sci. Technol., B* **1998**, *16*, 3142−3149.
(2) Ito, T.; Okazaki, S. *Nature* **2000**, *406*, 1027−1031.
(3) Yang, P. D.; Wirnsberger, G.; Huang, H. C.; Cordero, S. R.; McGehee, M. D.; Scott, B.; Deng, T.; Whitesides, G. M.; Chmelka, B. F.; Buratto, S. K.' Stucky, G. D. *Science* **2000**, *287*, 465−467.
(4) Xia, Y. N.; Kim, E.; Zhao, X. M.; Rogers, J. A.; Prentiss, M.; Whitesides, G. M. *Science* **1995**, *273*, 347−349.
(5) Xia, Y. N.; Rogers, J. A.; Paul, K. E.; Whitesides, G. M. *Chem. Rev.* **1999**, *99*, 1823−1848.
(6) Chou, S. Y.; Krauss, P. R.; Renstrom, P. J. *Science* **1996**, *272*, 85−87.
(7) Chou, S. Y.; Keimel, C.; Gu, J. *Nature* **2002**, *417*, 835−837.
(8) Chou, S. Y.; Krauss, P. R.; Zhang, W.; Guo, L. J.; Zhuang L. *J. Vac. Sci. Technol.* **1997**, *15*, 2897−2904.
(9) Albrecht, M.; Rettner, C. T.; Moser, A.; Best, M. E.; Terris, B. D. *Appl. Phys. Lett.* **2002**, *81*, 2875−2877.
(10) Piner, R. D.; Zhu, J.; Xu, F.; Hong, S. H.; Mirkin, C. A. *Science* **1999**, *283*, 661−663.
(11) Redon, C.; Brochard-wyart, F.; Rondelez, F. *Phys. Rev. Lett.* **1991**, *66*, 715−718.
(12) Herminghaus, S.; Jacobs, K.; Meche, K.; Bischof, J.; Fery, A.; Ibn-Elhaj, M.; Schlagowski, S. *Science* **1998**, *282*, 916−919.
(13) de Gennes, P. G. *Rev. Mod. Phys.***1985**, *57*, 827−863.
(14) Srolovitz, D. J.; Goldiner, M. G. *J. Met.* **1995**, *3*, 31.
(15) Bischof, J.; Scherer, D.; Herminghaus, S.; Leiderer, P. *Phys. Rev. Lett.* **1996**, *77*, 1536−1539.
(16) Higgins, A. M.; Jones, A. L. *Nature* **2000**, *404*, 476−478.
(17) Huang, J.; Kim, F.; Tao, A. R.; Connor, S.; Yang, P. D. *Nat. Mater.* **2005**, *4*, 896−900.
(18) Keene, B. J. *Int. Mater. Rev.* **1993**, *38*, 157−192.
(19) Brandes, E. A. *Smithells Metal Reference Book*, 6th ed.; Butterworth: London, 1983.
(20) Hu, X. Y.; Cahill, D. G.; Averback, R. S. *Appl. Phys. Lett.* **2000**, *76*, 3215−3217.
(21) Hu, X. Y.; Cahill, D. G.; Averback, R. S. *J. Appl. Phys.* **2001**, *89*, 7777−7783.
(22) Plateau, J. *Transl. Annu. Rep. Smithsonian Inst.* **1873**, 1863.
(23) Rayleigh, L. *Proc. London Math. Soc.* **1987**, *10*, 4.
(24) Nichols, F. A.; Mullins, W. W. *Trans. Metall. Soc. AIME* **1965**, *233*, 1840.
(25) Tiunuk Molares, M. E.; Balogh, A. G.; Cornelius, T. W.; Neumann, R.; Trautmann, C. *Appl. Phys. Lett.* **2004**, *85*, 5337−5339.
(26) Oechsner, H. *Appl. Phys.* **1975**, *8*, 185−198.
(27) Sigmund, P. *J. Mater. Sci.* **1973**, *8*, 1545−1553.
(28) Yang, B.; Liu, F.; Lagally, M. G. *Phys. Rev. Lett.* **2004**, *92*, 025520.
(29) Karmous, A.; Cuenat, A.; Ronda, A.; Berbezier, I.; Atha, S.; Hull, R. *Appl. Phys. Lett.* **2004**, *85*, 6401−6403.
(30) Cuenat, A.; George, H. B.; Chang, K. C.; Blakely, J. M.; Aziz, M. J. *Adv. Mater.* **2005**, *17*, 2845−2849.
(31) Gierak, J.; Mailly, D.; Hawkes, P.; Jede, R.; Bruchhaus, L.; Prével, B.; Mélinon, P.; Perez, A.; Hyndman, R.; Jamet, J.-P.; Ferré, J.; Mougin, A.; Chappert, C.; Mathet, V.; Warin, P.; Chapman *J. Appl. Phys. A* **2005**, *80*, 187−194.
(32) Pászti, Z.; Petó, G.; Horváth, Z. E.; Geszti, O.; Karacs, A.; Guczi, L. *Appl. Phys. A* **2003**, *76*, 577−587.
(33) Ishitani, T.; Koike, H.; Yaguchi, T.; Kamino, T. *J. Vac. Sci. Technol., B* **1998**, *16*, 1907−1913.
(34) *Ion Implantation*; Ryeesl, H., Ruge, I., Eds.; John Wiley & Sons: New York, 1986; pp 91−94.


NL060492Z